INSTITUTE OF PHYSICS PUBLISHING MODELLING AND SIMULATION IN MATERIALS SCIENCE AND ENGINEERING

Modelling Simul. Mater. Sci. Eng. **15** (2007) 121–134 doi:10.1088/0965-0393/15/2/008

Two-phase modelling of hot tearing in aluminium alloys using a semi-coupled approach

V Mathier[1], J-M Drezet[1,2] and M Rappaz[1]

[1] Computational Materials Laboratory, Ecole Polytechnique Fédérale de Lausanne, Station 12, Lausanne CH-1015, Switzerland
[2] Calcom-ESI SA, Parc Scientifique, EPFL, Lausanne CH-1015, Switzerland

E-mail: vincent.mathier@epfl.ch

Received 16 August 2006, in final form 11 January 2007
Published 5 February 2007
Online at stacks.iop.org/MSMSE/15/121

Abstract

Hot tearing, one of the most severe defects observed in castings, is due to both tensile stresses and lack of interdendritic liquid feeding in the mushy zone. In order to predict this phenomenon, the two-phase averaged conservation equations for mass and momentum must be solved in the mushy region of the material. In recent contributions, M'Hamdi *et al* (2002 *Metall. Mater. Trans.* A **33** 2081–93) proposed a strongly coupled resolution scheme for this set of equations. The solution of the mechanical problem is obtained using a rheological model established by Ludwig *et al* (2005 *Metall. Mater. Trans.* A **36** 1525–35). In the present contribution, the problem is addressed with a slightly different approach. The same rheological model is used for the solid skeleton (i.e. saturated porous medium treatment), but the influence of liquid pressure is neglected at this stage. This assumption allows for a weakly coupled resolution scheme in which the mechanical problem is first solved alone using ABAQUS® and user subroutines. Then, the liquid pressure is calculated separately accounting for the viscoplastic deformation of the porous solid and solidification shrinkage. This is done with a code previously developed for porosity calculations which uses a refined mesh in the mushy zone (Pequet *et al* 2002 *Metall. Mater. Trans.* A **33** 2095–106). The stability of the numerical tools is presented and the modelling approach is then applied to a virtual experiment. Finally, two approaches are examined to study the hot tearing tendency in this problem.

1. Introduction

Together with porosity, hot tearing is one of the most important defects that may form in castings during solidification. Upon cooling, large cracks spontaneously appear in the mushy alloy causing significant productivity losses. These tears correspond to the tensile failure of

the mushy alloy at high solid fractions (typically 90–95%). This defect is attributed to the conjunction of thermal strains driving the cracking process and hindered liquid flow, which prevents any void from being filled with liquid. If the solid fraction is below the typical range, liquid will flow easily in between the solid grains and 'heal' initiated cracks by flowing into the void. On the other hand, at solid fractions above typically 96%, the solid network becomes coalesced (the remaining liquid is found as isolated droplets) and thus behaves like a dense solid able to withstand tensile or shear stresses imposed by the process.

In order to be able to assess hot tearing quantitatively, it is thus necessary to consider both liquid flow and straining in a mushy material. For this complex purpose, efficient numerical modelling tools are required to obtain an accurate thermomechanical description of the solidification process. Once such results are available, it is customary to define a criterion to indicate the hot tearing susceptibility of a given alloy under given processing conditions. A review of the most classical criteria is given in [1].

The coupling between strains and liquid feeding deep in the mushy zone was modelled by several authors with the objective of predicting defect formation. A first approach was developed by Rappaz *et al* while establishing the RDG criterion [2]. This model is derived assuming a simplified strain state (uniform strain rate perpendicular to primary dendrite arms) and describes how a void (tear) can nucleate in the mushy zone using a critical liquid pressure drop. More recently M'Hamdi *et al* [3] provided a method for solving the fully coupled problem taking into account the complex rheology of the mushy alloy. From the physics standpoint, this approach is close to the RDG criterion but it allows for a more accurate description of the strains development in a cast part during an actual process.

This paper presents a semi-coupled method for solving the mechanical and fluid flow problems. Its main drawback is that it is not strongly coupled (as opposed to [3]) but the different orders of magnitude of stresses between the solid and the liquid are expected to minimize this problem. On the other hand, it offers significant advantages since it is easier to implement and allows the use of specialized codes to obtain more accurate solutions to the mechanical (ABAQUS®) and liquid pressure (ProCAST®) problems. The present method is applicable to standard processes in the aluminium industry, such as dc casting. The governing equations are first summarized together with relevant assumptions and the mechanical behaviour is then characterized. Finally, numerical convergence studies as well as an application problem are described and the results are discussed.

2. Two-phase modelling

2.1. Averaged equations

The model involves momentum and mass conservation in a mushy zone (a mixture of solid and liquid phases) containing a volume fraction of solid g_s. The two-phase mass conservation equation is expressed under the following form [4]:

$$\frac{\partial}{\partial t}(g_s\rho_s + g_l\rho_l) + \nabla \cdot (g_s\rho_s\boldsymbol{v}_s + g_l\rho_l\boldsymbol{v}_l) = 0, \tag{1}$$

where g is the volume fraction, ρ the density, $\boldsymbol{v}$ the velocity and the s (respectively, l) subscript refers to the solid (respectively, liquid) phase. The flow of a liquid with viscosity μ in a porous medium (i.e. the solid skeleton) of permeability K is described using Darcy's law:

$$g_l(\boldsymbol{v}_l - \boldsymbol{v}_s) = -\frac{K}{\mu}(\nabla p_l - \rho_l \boldsymbol{g}), \tag{2}$$

where $\boldsymbol{g}$ is the gravity vector and p_l the pressure in the liquid phase. This can be substituted in the mass conservation equation thus giving [3]

$$\frac{\partial \rho}{\partial t} + \nabla \cdot (\rho \boldsymbol{v}_\mathrm{s}) - \nabla \left(\frac{\rho_\mathrm{l} K}{\mu} (\nabla p_\mathrm{l} - \rho_\mathrm{l} \boldsymbol{g}) \right) = 0, \tag{3}$$

where the average density $\rho = g_\mathrm{s}\rho_\mathrm{s} + g_\mathrm{l}\rho_\mathrm{l}$ has been introduced. The average momentum conservation equation can be derived along similar lines [3,4]. The averaged stress tensor is expressed under the assumption that the liquid does not bear significant shear stresses:

$$\nabla \cdot \boldsymbol{\sigma} + \rho \boldsymbol{g} = 0 \Leftrightarrow \nabla \cdot (g_\mathrm{s}\boldsymbol{\sigma}_\mathrm{s} - g_\mathrm{l} p_\mathrm{l} \boldsymbol{I}) + \rho \boldsymbol{g} = 0, \tag{4}$$

where $\boldsymbol{I}$ is the unit tensor, $\boldsymbol{\sigma}_\mathrm{s}$ is the stress in the solid and $\boldsymbol{\sigma}$ is the total stress. In the framework of saturated porous media theory, it is customary to introduce the effective stress $\boldsymbol{\sigma}_\mathrm{eff}$ (total stress minus hydrostatic liquid contribution) and to rewrite the equation as

$$\boldsymbol{\sigma}_\mathrm{eff} = \boldsymbol{\sigma} + p_\mathrm{l}\boldsymbol{I} \Rightarrow \nabla \cdot \boldsymbol{\sigma}_\mathrm{eff} + \rho \boldsymbol{g} = \nabla p_\mathrm{l}. \tag{5}$$

The problem consists of solving equations (3) and (5) for displacements in the solid and pressure in the liquid. These two unknowns are involved in both the equations (solid displacements are related to stresses through the constitutive law), which means that they are coupled.

In this work, a model valid for most of the common solidification processes in which hot tearing is observed (continuous casting, gravity die casting, laser welding, etc.) will be established. In these cases, only the atmospheric pressure is exerted on the liquid and the metallostatic head remains small. Moreover, pressure drops across the mushy zone are typically of the order of a few tens of kPa. On the other hand, stresses caused by inhomogeneous thermal strains are of the order of MPa. These considerations suggest that it is reasonable to neglect the liquid pressure contribution to the effective stress. We will thus assume that the two-phase momentum conservation equation may be written as

$$\nabla \cdot \boldsymbol{\sigma} + \rho \boldsymbol{g} = 0. \tag{6}$$

This assumption was validated through test cases run on the Tearsim® software [5] in which fully or weakly coupled resolution schemes can be alternatively selected. Under this condition, the problem can be solved in a weakly coupled manner since equation (6) can be solved alone for solid displacements. The results of this calculation ($\boldsymbol{v}_\mathrm{s}$ field) may then be used as input when solving equation (3) for the liquid pressure.

2.2. *Rheology*

Solving equation (6) is possible provided a suitable constitutive law relating stresses to strains (and thus to solid displacements) is available. For the case of a mushy zone at sufficiently high solid fraction (coherency is reached typically above 65%), Ludwig *et al* [6] formulated a rheological model that captures two very important aspects. On one hand, the mushy zone is a mixture of two incompressible phases with different densities. As a consequence, it is compressible (its density may vary with the applied stress) and this must be taken into account. Moreover, the presence of the liquid phase disturbs the continuity of the solid making it only partially cohesive, i.e. strains are not fully transmitted across the solid phase. This model is expressed in the following form (please note that the assumption that $\boldsymbol{\sigma}_\mathrm{eff} \approx \boldsymbol{\sigma}$ was introduced):

$$\dot{\varepsilon}^\mathrm{vp} = \frac{\dot{\varepsilon}_0}{(Cs_0)^n} \left(A_2 P_\mathrm{s}^2 + A_3 \sigma_M^2 \right)^{\frac{n-1}{2}} \left(-\frac{A_2}{3} P_\mathrm{s} \boldsymbol{I} + \frac{3}{2} A_3 \boldsymbol{S} \right) = \dot{\varepsilon}_\mathrm{sw} \boldsymbol{I} + \frac{3}{2} \frac{\dot{\varepsilon}_\mathrm{cr}}{\sigma_M} \boldsymbol{S}, \tag{7}$$

where $\dot{\varepsilon}_{ij}^\mathrm{vp} = \frac{1}{2}\left((\partial (\boldsymbol{v}_\mathrm{s})_i)/(\partial x_j) + (\partial (\boldsymbol{v}_\mathrm{s})_j)/(\partial x_i) \right)$ is the viscoplastic strain rate tensor, $\dot{\varepsilon}_\mathrm{sw}$ and $\dot{\varepsilon}_\mathrm{cr}$ are the volumetric (swelling in ABAQUS®) and deviatoric (creep in ABAQUS®) equivalent

strain rates, $P_s = -\frac{1}{3}\mathrm{tr}(\boldsymbol{\sigma})$ is the pressure in the solid[3], s_0 is a material constant that indicates its resistance to stress, $\boldsymbol{S} = \boldsymbol{\sigma} + P_s\boldsymbol{I}$ is the deviatoric stress tensor and σ_M its second invariant ($\sigma_M^2 = \frac{3}{2}\boldsymbol{S} : \boldsymbol{S}$). C is the cohesion internal variable, which varies from zero (freely floating solid grains in liquid) to one (dense solid or fully coalesced granular skeleton). Additional closing relations are

$$\dot{\varepsilon}_0 = A\exp\left(-\frac{Q}{RT}\right) \qquad A_2 = \frac{9}{4}\left\{n\left[(1-g_s)^{-\frac{1}{n}} - 1\right]\right\}^{\frac{-2n}{n+1}} \qquad A_3 = \left[1 + \frac{2}{3}(1-g_s)\right](g_s)^{\frac{-2n}{n+1}}. \tag{8}$$

The model is completed by an evolution equation for the internal variable C [6]:

$$\frac{\mathrm{d}C}{\mathrm{d}t} = \alpha\left(1 - \frac{C}{C^*}\right)\sqrt{\frac{2}{3}\dot{\varepsilon}^{\mathrm{vp}} : \dot{\varepsilon}^{\mathrm{vp}}}. \tag{9}$$

Introducing the triaxiality $X = (P_s)/(\sigma_M)$ (<0 in tension), the following relations are adopted:

$$\begin{aligned} &\alpha(g_s, X \geqslant 0) = \alpha_0 + \alpha_1 \frac{g_s^{\frac{1}{3}}}{1-g_s^{\frac{1}{3}}} \qquad && \alpha\,(g_s, X < 0) = \alpha_0 + \alpha_1 \frac{g_s^{\frac{1}{3}}}{1-g_s^{\frac{1}{3}}} \exp\left[k\left(g_s - g_s^{\mathrm{coal}}\right)\right], \\ &C^*\,(g_s, X > 2) = 1 && C^*\,(g_s, X \leqslant 2) = 1 - (1-g_s)^p\,. \end{aligned} \tag{10}$$

These expressions take into account the dependence of the mushy zone behaviour on the stress state. Moreover, the effect of coalescence of the grains at high solid fractions [7–9] is introduced above a critical fraction g_s^{coal} of typically 96%. The materials parameters (activation energy Q, constants A, k, α_0 and α_1, exponents p and n) that appear in this model were determined by experimental identification [6, 10, 11].

In the case of the fully solid material ($g_s = 1, C = 1$), the model takes a more classical form:

$$\dot{\varepsilon}^{\mathrm{vp}} = \frac{3}{2}\frac{\dot{\varepsilon}_{\mathrm{cr}}}{\sigma_M}S \qquad \text{with } \dot{\varepsilon}_{\mathrm{cr}} = \frac{\dot{\varepsilon}_0}{s_0^n}\sigma_M^n. \tag{11}$$

This expression for the equivalent creep rate $\dot{\varepsilon}_{\mathrm{cr}}$ is known to model well the behaviour of aluminium alloys above 400 °C under relatively low stresses. At lower temperatures, the following formulation should be used:

$$\sigma_M = \kappa(T)\varepsilon_{\mathrm{cr}}^{\eta(T)}\left(\frac{\dot{\varepsilon}_{\mathrm{cr}}}{\dot{\varepsilon}_{\mathrm{u}}}\right)^{\lambda(T)} \qquad \text{with } \varepsilon_{\mathrm{cr}} = \int_{t(T\leqslant T_0)}^{t} \dot{\varepsilon}_{\mathrm{cr}}\,\mathrm{d}t \;\text{ and }\; \dot{\varepsilon}_{\mathrm{u}} = 1\,\mathrm{s}^{-1}, \tag{12}$$

where κ, η and λ are temperature-dependent parameters to be determined experimentally and T_0 is the temperature below which strain hardening becomes significant (dynamic recovery is very fast above T_0) [11].

2.3. Liquid behaviour

The liquid phase is Newtonian and is characterized by a viscosity μ. The temperature dependence of μ was neglected in the present work. This liquid flows within the mushy zone, whose permeability is described by the Karman–Cozeny relationship:

$$K = \frac{(1-g_s)^3}{g_s^2}\frac{\phi^2}{180}, \tag{13}$$

where ϕ is the grain diameter (the alloy is assumed to be grain-refined leading to a globular microstructure).

[3] Please note that this is the pressure experienced locally in the solid phase. The liquid pressure p_l introduced before is the local pressure in the liquid phase. These two pressures may have different values. In fact, it is the normal stress that must be continuous at the solid–liquid interface. The difference between P_s and p_l can thus be attributed to capillarity, liquid flow and mostly to the deviatoric stress (in the solid) component normal to this interface.

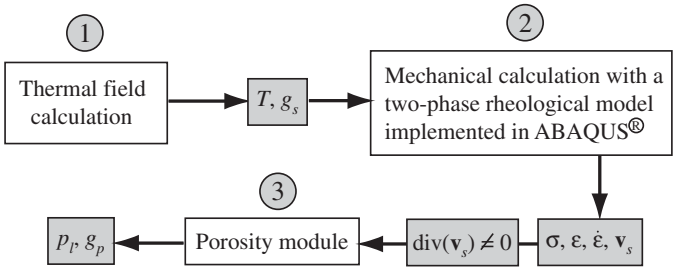

Figure 1. Flow chart for the sequentially coupled calculation.

3. Numerical tools

3.1. Implementation

The mechanical calculations are performed using the ABAQUS® package, which solves equation (6) using a finite element method. The most critical point is to specify the material behaviour for any temperature. According to experimental data, the elastic modulus decreases with temperature and takes a low value (typically 0.1 GPa) when the solid fraction is below 70%. The liquid and incoherent mush are thus approximated as an elastic solid with low modulus. This assumption proved satisfactory from both the points of view of physical relevance and numerical convergence. For $g_s > 65\%$ and $T > 400\,^{\circ}\mathrm{C}$, equations (7) and (9) were implemented. As a consequence, the dense solid behaviour above 400 °C is described by equation (11). Finally, the dense solid below 400 °C is described by equation (12). Mechanical properties for a full range of temperature are thus described (through the CREEP user function). Moreover, following [12], the thermal expansion coefficient is taken equal to zero for $g_s < 80\%$ (while it is around $25 \times 10^{-6}\,\mathrm{K}^{-1}$ in the solid state).

The liquid pressure problem described by equation (3) is solved using the porosity module developed by Pequet and coworkers [13, 14] and available in ProCAST®. It involves a mushy zone refinement technique, which proves very useful for large problems, and a finite volume resolution method.

A set of input/output tools has also been set up in order to follow the flow chart presented in figure 1. First of all, the temperature and solid fraction fields are obtained from the finite element package ProCAST® under the correct boundary conditions (please note that the solidification path $g_s(T)$ is provided as input). The results are then fed into the mechanical solver through the UTEMP user function. ABAQUS® provides the values of thermal stresses, strains and strain rates, which may be relevant in formulating hot tearing criteria. The last step consists of taking the solid velocity field calculated by ABAQUS® as input to the porosity module, which calculates pressure in the liquid p_l. Note that this module also calculates the fraction of porosity g_p with the model described in [13, 14].

3.2. Convergence study

Before applying the modelling approach to actual processes, it is important to study the accuracy of the solvers and to determine a suitable range for numerical parameters such as time step (Δt) or mesh size (Δx). The mechanical model was tested for a tensile test on a cylindrical bar (AA5182 alloy) 1 cm in radius and 20 cm long. The temperature field varies linearly from a hot spot in the centre to colder ends (the 20 K difference resulting in a symmetric temperature gradient of $2\,\mathrm{K\,cm}^{-1}$). The cooling rate is kept constant at $-1.5\,\mathrm{K\,s}^{-1}$ for 100 s so

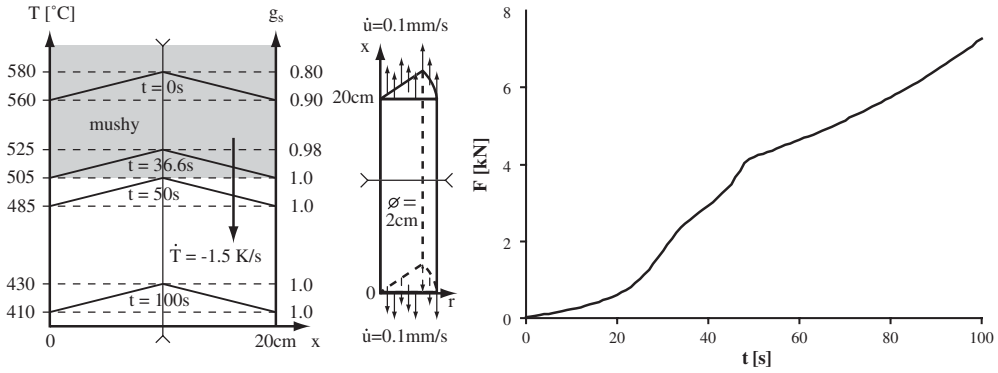

Figure 2. Conditions for the mechanical solver benchmark test and computed force response for the reference calculation ($\Delta x = 1$ mm and $\chi = 10^{-8}$ ($\Delta t = 0.01$ s)).

that the sample is tested over a wide behaviour range (mushy, hot and cold solid). A constant displacement rate of 0.1 mm s^{-1} (i.e. mean strain rate of 10^{-3} s^{-1}) is applied to both ends of the sample during the entire test. These conditions are summarized in figure 2.

The force response as a function of time is used to characterize the test. Another useful quantity is the cumulated volumetric viscoplastic strain CESW $= \int_0^t \mathrm{tr}(\dot{\varepsilon}^{\mathrm{vp}})\,\mathrm{d}t$, which is a characteristic of the mushy zone behaviour. Several calculations were performed for different mesh sizes (square axisymmetric elements were used) and time steps.

The material properties are heavily dependent upon the solid fraction, which leads to a highly nonlinear problem. This is most generally the case when dealing with the mechanical behaviour of a mushy zone. Moreover, numerous physical parameters play a role in such a problem (stress, strain, temperature, history, etc). In order to solve such a problem accurately (i.e. determine a stress response in a viscoplastic material under an applied strain rate), it is necessary to use a relatively small time step. In the present case, it is very difficult to find a single material parameter that would allow determining the time step. It is more relevant to ensure that the solution of the problem is not varying too rapidly from one step to another. In this case, the imposed strain rate may be decomposed into elastic and viscoplastic contributions: $\dot{\varepsilon} = \dot{\varepsilon}_{\mathrm{el}} + \dot{\varepsilon}_{\mathrm{cr}}$. The strain increment (which is known since the displacement is imposed) during one time step is then $\Delta\varepsilon = \dot{\varepsilon}\Delta t = \Delta\varepsilon_{\mathrm{el}} + \Delta\varepsilon_{\mathrm{cr}}$. The stress response is obtained from the elastic strain and elasticity constants: $\Delta\sigma = E\Delta\varepsilon_{\mathrm{el}}$. If the viscoplastic strain rate is constant, $\Delta\varepsilon_{\mathrm{cr}}$ is calculated accurately and the right stress may be obtained for any time step. In real problems, $\dot{\varepsilon}_{\mathrm{cr}}$ changes with time and its variation during one time step should be kept to an acceptable low value. This variation can be measured by the χ parameter, defined as follows:

$$\chi = (\dot{\varepsilon}_{\mathrm{cr}}|_{t+\Delta t} - \dot{\varepsilon}_{\mathrm{cr}}|_t)\Delta t. \tag{14}$$

When solving this problem, the time step should be selected so that χ remains small when compared with $\Delta\varepsilon_{\mathrm{el}}$. This procedure is implemented in ABAQUS® (where χ is known as the CETOL parameter) [15]. The value of χ is usually taken to be constant and Δt thus varies throughout the calculation. An indicative value of the average time step will be given in brackets after the displayed values of χ. The first objective was to determine how small χ should be in order to obtain stable solutions.

The force response as a function of time was first simulated (figure 2) with $\Delta x = 1$ mm and $\chi = 10^{-8}$ ($\Delta t = 0.01$ s). This is the most precise calculation that was conducted and this result will be used as a reference since no analytical solution can be found for this problem. It

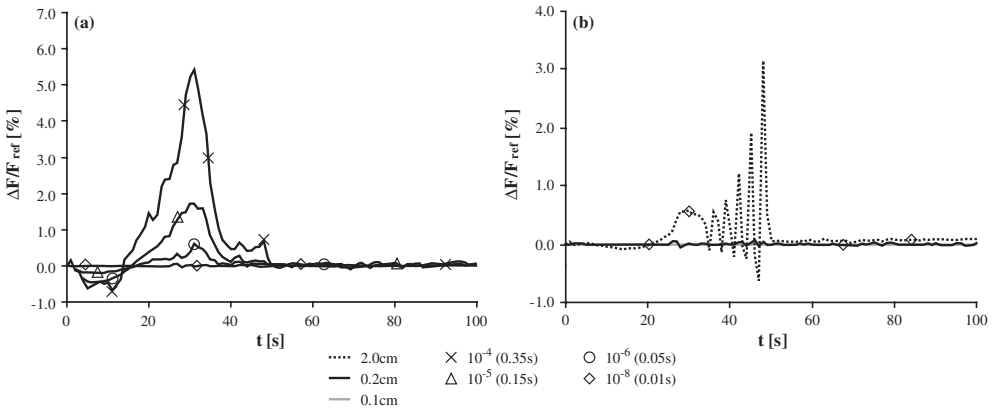

Figure 3. Relative differences between the calculated (with Δx and χ (Δt)) force response and the reference solution. Different lines correspond to different mesh sizes while symbols indicate various time steps. (*a*) The time step effect for $\Delta x = 0.2$ cm; (*b*) the mesh size effect for $\chi = 10^{-8}$ (0.01 s).

was checked that this solution is independent of the time step (i.e. smaller values of χ did not lead to another solution).

Figure 3 displays the relative difference in the computed reaction force between the reference and the cases with varying Δx and χ (Δt). Figure 3(*a*) shows the effect of the time step when $\Delta x = 2$ mm. The reference solution is essentially recovered for $\chi = 10^{-8}$ (0.01 s). As χ is increased to 10^{-6} (0.05 s), 10^{-5} (0.15 s) and 10^{-4} (0.35 s), the error increases up to 6% in the mushy region but remains negligible when $t > 50$ s (fully solidified material). This order of precision is acceptable for full scale calculations. However, if χ is set to 10^{-3} (0.45 s) or above, the error peaks to around 15% in the mushy alloy and is close to -3.5% in the solid. This is not satisfactory and the χ value was kept to 10^{-4} or below in further calculations. Please note that other calculations were conducted for different values of imposed strain rate, thermal gradient and cooling rate. It was found that using $\chi < 10^{-4}$ led to satisfactory results in all the cases and seems to be a reasonable criterion to be used in more complex situations.

While the time step appears to have a significant effect on the force response, this is not the case for the mesh size as suggested by figure 3(*b*). For the same time step, the force response for different Δx (1 mm, 2 mm or 2 cm) is very similar. The most significant effect is the appearance of oscillations for the very coarse mesh ($\Delta x = 2$ cm) during the mushy to solid transition. These fluctuations remain however clearly below 4% and are not too much of a concern at this stage.

Figure 4 shows the cumulated volumetric strain (CESW) profile in the longitudinal direction after the test. Again, the CESW value is given for the most refined solution while the other calculation results are shown as a relative difference for this reference. The calculation with $\Delta x = 1$ mm (same as reference) and $\chi = 10^{-4}$ (0.35 s) indicates that the time step has relatively little influence since the absolute error is less than 4% (neglecting the -20% obtained at the edge of the specimen, where CESW is very small). As long as χ is less or equal to 10^{-4}, the time step effect is noticeable but remains acceptable (again, less restrictive tolerance values lead to inaccurate results). The effect of the mesh size is illustrated by the results for $\Delta x = 2$ mm and 2 cm ($\chi = 10^{-8}$, same as reference). If the mesh is coarsened slightly, the effect is not important (the variation of CESW within one element remains small) while it becomes dramatic for the 2 cm mesh. This shows that a mesh adapted to model the

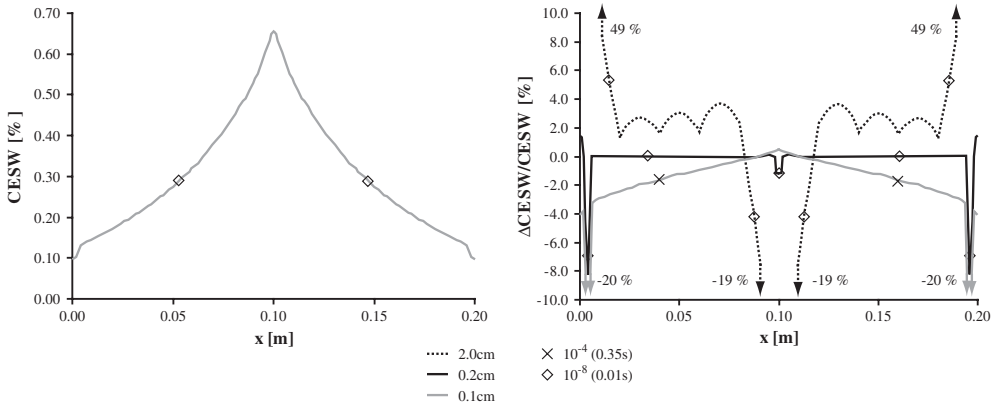

Figure 4. Cumulated volumetric strain (CESW) profile at the end of the mechanical test. The reference solution (with $\Delta x = 0.1$ cm mesh and $\chi = 10^{-8}$ (0.01 s)) is displayed on the left while the plot on the right contains relative differences between other cases and this reference. Different lines correspond to different mesh sizes while symbols indicate various time steps.

force response accurately may not be as efficient to capture everything that happens in the mushy zone.

The liquid pressure calculation was benchmarked using a one-dimensional case for which an analytical solution exists. It consists of a Bridgman-type experiment under steady conditions in which isotherms move at a velocity $v_T = 1.4\,\mathrm{mm\,s^{-1}}$. The thermal gradient G is $1000\,\mathrm{K\,m^{-1}}$ and the liquid fraction is assumed to vary linearly with temperature ($g_\mathrm{l} = 1 - g_\mathrm{s} \propto x \propto T$) over a solidification interval ΔT_s of 100 °C. It was assumed that the mushy zone has a constant and uniform characteristic length scale $\phi = 25\,\mu$m.

For this case, an analytical solution for the liquid pressure profile in the mushy zone can be adapted from Niyama *et al* [16]:

$$p_\mathrm{l}(g_\mathrm{l}(x)) = p_\mathrm{ref} - \int_1^{g_\mathrm{l}} \mu\beta \frac{v_T}{G} \Delta T_\mathrm{s} \frac{180}{\phi^2} \frac{(1-g_\mathrm{l})^2}{g_\mathrm{l}^2}\,\mathrm{d}g_\mathrm{l} = p_\mathrm{ref} - \Omega\left(-\frac{1}{g_\mathrm{l}} - 2\ln(g_\mathrm{l}) + g_\mathrm{l}\right), \tag{15}$$

where μ is the liquid viscosity (taken as 10^{-3} Pa s for liquid aluminium), $\beta = (\rho_\mathrm{s})/(\rho_\mathrm{l}) - 1$ is the shrinkage factor (8.3% was taken in this test), $\Omega = (180\,\mu\beta v_T \Delta T_\mathrm{s})/(G\phi^2)$ and p_ref is the sum of the atmospheric pressure and the metallostatic head.

Figure 5 displays the liquid pressure profile across the mushy zone as a function of the solid fraction for different cell sizes (Δx) and time steps (Δt, which is constant and determined by the user in this case). A 'cell' is one cubic element of the structured mesh generated in the mushy zone refinement technique [13]. These results indicate that coarse meshes will cause the calculated pressure to drop too rapidly as the solid fraction increases. As the mesh is refined, the profile converges to the analytical solution for the entire mushy zone (a eutectic fraction of 2% was assumed for these calculations so that no liquid remains above $g_\mathrm{s} = 0.98$). This shows that the porosity module yields accurate results even though the fully solid boundary condition is treated by a penalty approximation as detailed in [13]. The time step effect is more difficult to discuss since it does not have a marked effect on the pressure profile as long as $(v_T \Delta t)/(\Delta x) < 1$. In general, a finer time step will help to prevent oscillations that can appear in the solution. As a guideline, it was found that a fairly stable solution is obtained by

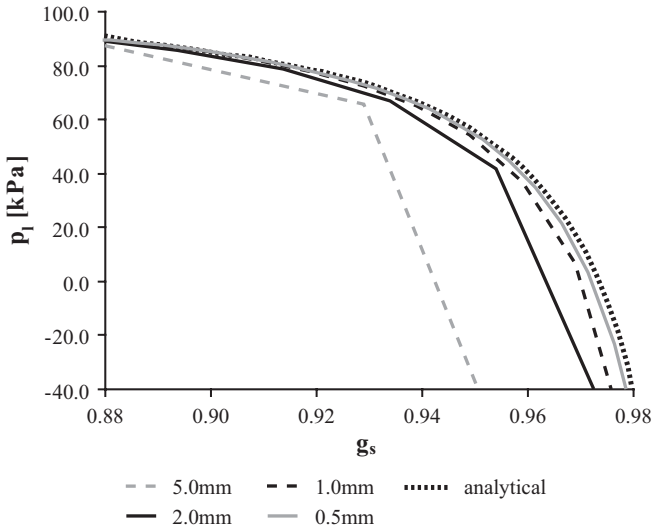

Figure 5. Liquid pressure profiles across the mushy zone for $\Delta t = 0.05$ s. The line type indicates the different cell sizes and the analytical profile is also displayed for reference.

selecting a cell size Δx so that g_s changes by 1% or less within the cell. Then, the time step Δt should be selected according to $(v_T \Delta t)/(\Delta x) \leqslant 0.2$.

Both these benchmark problems show that reasonably accurate solutions can be obtained for numerical parameters in a range of values that can be used for larger simulations. In the next section, the semi-coupled approach is applied to a more relevant problem involving both fluid flow and solid deformation.

4. Application problem

4.1. Virtual restrained solidification test

The semi-coupled approach was applied to a virtual restrained solidification test in which hot tearing could also be studied (figure 6). The specimen is a cylinder with a gauge length of 10 cm and 2 cm diameter. It is notched at mid-height with an angle α and depth c. Two enlarged regions 4 cm in diameter are found at both ends so as to ensure the attachment of the sample to fixed copper jaws. The gauge length is contained in a steel mould and the notch region is covered with additional insulation to generate a hot spot. The symmetry of the problem allows simulating only half the height of the specimen using 2D axisymmetric elements in a longitudinal section.

Different convective heat transfer coefficients (for an external temperature of 20 °C) were assumed, i.e. $600\,\mathrm{W\,m^{-2}\,K^{-1}}$, $300\,\mathrm{W\,m^{-2}\,K^{-1}}$ and $5\,\mathrm{W\,m^{-2}\,K^{-1}}$ for the transfer through copper, steel and insulator, respectively. Mechanical boundary conditions are such that both ends of the sample are attached to the jaws, which are fixed and rigid. In this model experiment, liquid AA5182 alloy is poured at 680°C in the mould. It cools and solidifies according to the conditions described above. Thermal contraction of the sample gives rise to tensile stresses at the level of the notch, possibly inducing hot tearing.

Several calculations were conducted using the approach described above. Different notch shapes (no notch, $\alpha = 30°, 90°$, round notch) and lengths ($c = 0, 2.5, 5$ and 7.5 mm) were used.

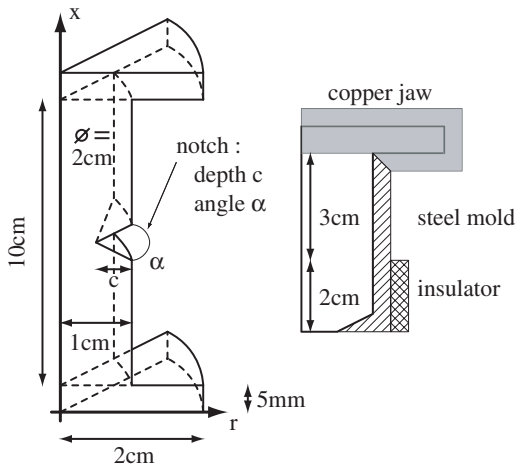

Figure 6. Conditions for the virtual restrained solidification test. The specimen geometry is shown on the left and the simulation domain together with thermal boundary conditions on the right.
(This figure is in colour only in the electronic version)

The thermal field was calculated for each case as well as the liquid pressure p_l^o (respectively, porosity fraction g_p^o, which is calculated assuming that 0.2 $cc_{STP}/100$ g of dissolved hydrogen is present in the melt) neglecting the effect of solid deformation. Mechanical calculations were then performed for each geometry and it was then possible to calculate the liquid pressure (respectively, porosity fraction) taking into account the effect of solid strains: p_l^{meca} (respectively, g_p^{meca}). This was done under the following assumption, which is relevant in this case: $\nabla \cdot (\rho \boldsymbol{v}_s) \approx \rho \cdot \mathrm{tr}(\dot{\varepsilon}^{vp})$. Each porosity calculation took about 7 h on an Intel Xeon @ 2 GHz while the resolution of the mechanical problem lasted about 6.5 h on a MIPS R14000 @ 450 MHz.

4.2. Hot tearing tendency assessment

In order to estimate what kind of notch would most efficiently promote hot tearing in this test, a quite classical approach was undertaken. The present hot tearing susceptibility indicator is very similar to that of M'Hamdi *et al* [17] with a slight modification of the nucleation criterion. First, deformation in the solid is neglected to calculate the liquid pressure. Then, strains are taken into account and a new liquid pressure field is obtained. The difference between these two solutions is defined as the mechanically induced liquid pressure drop ($\Delta p_l^m = p_l^o - p_l^{meca}$). Nucleation of a hot tear is related to this quantity reaching a critical value Δp_{crit} (2 kPa was chosen following [2]). Once the crack is nucleated, the tensile deformation that will accumulate up to a coalescence solid fraction, g_s^{coal}, (where hot tears can no longer develop since the liquid is only found in isolated droplets and are fixed to 98% in this study) is an indication of the local hot tearing tendency (HCS):

$$\mathrm{HCS} = \theta \int_{\Delta p_l^m = \Delta p_{crit}}^{g_s = g_s^{coal}} (\omega_{sw} \dot{\varepsilon}_{sw} + \omega_{cr} \dot{\varepsilon}_{cr})\, \mathrm{d}t, \tag{16}$$

where θ is equal to 1 when the local mean stress is tensile and 0 otherwise and ω_{sw} and ω_{cr} are weighing factors showing the relative importance of volumetric and deviatoric strain components, respectively (taken to be 1 and 0.2, respectively, in this study [17]).

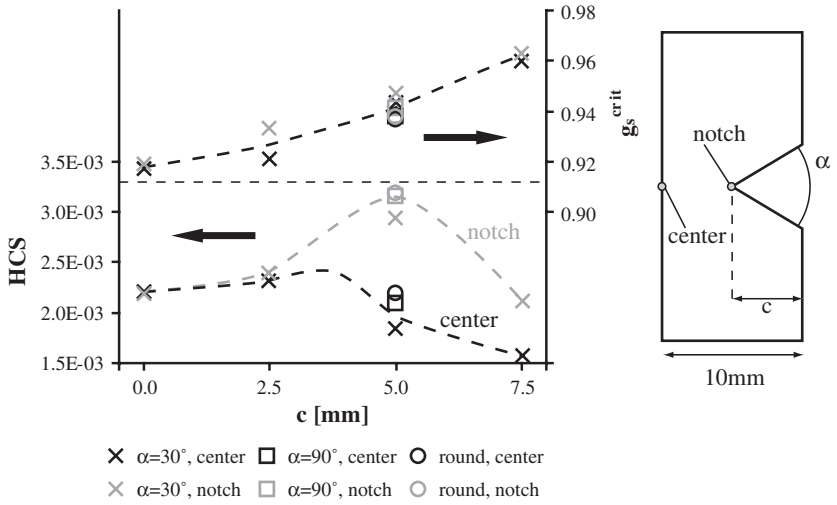

Figure 7. HCS (left) and solid fraction at nucleation g_s^{crit} (right) for different notches at the centre of the specimen and at the tip of the notch. Estimated tendencies are represented by dotted lines.

Figure 7 displays the final hot tearing susceptibility (HCS) for different notch sizes and shapes ($\alpha = 30^\circ$ and 90° as well as the result for a round notch of radius c). The HCS value was calculated on the horizontal symmetry plane (notch plane) at the centre of the specimen and at the tip of the notch. These values, which occupy the bottom half of the plot, are better discussed provided the critical solid fraction, g_s^{crit} (upper part of the plot), is also displayed. This parameter corresponds to the solid fraction at which the nucleation criterion is reached: $\Delta p_l^m(g_s = g_s^{crit}) = \Delta p_{crit}$.

The value of g_s^{crit} increases monotonically with the notch depth, c, which indicates that a deeper notch delays the nucleation of the crack (liquid feeding is enhanced in the reduced cross section). On the other hand, the presence of a notch causes strain concentration, thus explaining why the HCS increases more rapidly once the defect has nucleated. In summary, the effect of the notch is the result of a balance between delayed nucleation and higher straining. This explains why there is an intermediate notch size for which the hot tearing susceptibility is at a maximum. The influence of the crack shape is weaker but a similar conclusion can be drawn. It seems indeed that sharp notches, which cause large strain concentration, also correspond to delayed nucleation and are then not the most critical. This shows that hot tearing should be analysed from both defect nucleation and damage accumulation viewpoints.

4.3. Fracture mechanics approach

For the case without a notch ($c = 0$), a refined mesh was introduced so as to have elements 200 μm wide and 130 μm high in the horizontal symmetry plane. In this plane, the growth of a crack, which is assumed to have a disc shape and radius a, could be simulated by removing the elements during the stress calculation (elements along the crack path are removed one after another with a frequency high enough to prevent any relaxation effect). With this method, the elastic strain energy (volume integral of elastic stress times the elastic strain) stored in the specimen can be calculated as a function of the size of the crack. The elastic energy restored upon cracking, G_{el}, can then be obtained.

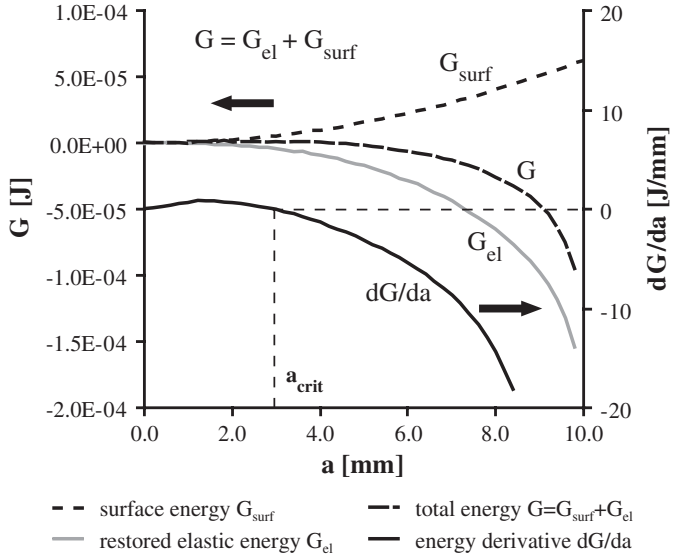

Figure 8. Determination of the critical defect size a_{crit} (case $c = 0$).

Classically, cracking may be analysed as a balance of restored strain energy versus created interface energy, G_{surf}. In hot tearing, cracks may propagate through the liquid phase without deformation of the solid grains at the crack tip. This process can be described with a brittle failure model where the surface energy is a simple function of the crack length: $G_{\text{surf}} = 2\gamma\pi a^2$, where γ is the new interface energy (a value of $0.9\,\text{J}\,\text{m}^{-2}$ was used so as to model the change from an intergranular liquid film to a crack). As in Griffith's analysis, there exists a critical crack radius a_{crit} (figure 8) such that $\left.\frac{\text{d}(G_{\text{el}}+G_{\text{surf}})}{\text{d}a}\right|_{a_{\text{crit}}} = 0$, i.e. any crack larger than a_{crit} will cause a catastrophic failure of the part.

The critical defect size, a_{crit}, was calculated for different assumed nucleation times. The value of a_{crit} is plotted in figure 9 as a function of the average solid fraction in the crack plane when the crack is nucleated. Up to a solid fraction of about 96%, the critical defect size is almost equal to the specimen size. This means that there is not enough elastic energy stored to cause a catastrophic failure of the mushy material. In this case fracture can only progress when sufficient damage (voiding) has accumulated at the crack tip. This is typical of a ductile fracture mode, which may be a relatively slow process. For $g_{\text{s}} > 96\%$, the amount of energy restored upon crack advance becomes significant and the critical defect size for fragile fracture decreases. However, in this solid fraction range, coalescence of solid grains occurs and the mushy alloy is no longer fragile (cracking must progress by deforming and breaking solid bridges). This will increase G_{surf}, greatly causing the critical defect size to remain very high. This indicates again that a failure process observed at such solid fractions is again more likely to be related to damaging mechanisms. Such conclusions could also be drawn when a displacement rate (tensile loading) was imposed on the copper jaws and would be even more true if crack tortuosity effects were taken into account.

These results show that classical fracture mechanics is probably not the best approach to obtain reliable hot tearing predictions. More accurate criteria will be obtained by considering ductile fracture modes. This problem could for example be studied through the concept of mechanically induced voiding: $\Delta g_{\text{p}}^{\text{m}} = g_{\text{p}}^{\text{meca}} - g_{\text{p}}^{\text{o}}$. This quantity is available in the current

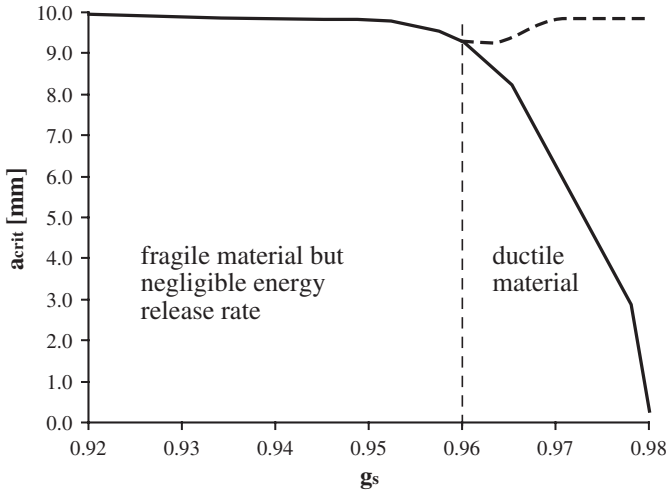

Figure 9. Critical defect size as a function of average solid fraction in the crack plane. Present results (solid line, fragile model) are given together with the proposition of a more accurate model at high solid fractions (dashed line).

framework, similarly to the mechanically induced pressure drop that was introduced to define the nucleation criterion in the definition of the HCS. It could be used to quantify a ductile fracture process based on damage accumulation as was proposed by Monroe and Beckermann in [18].

5. Conclusion

A semi-coupled method for describing quantitatively the mechanical and liquid flow conditions in the mushy zone under typical solidification processes conditions for aluminium alloys is presented. It shows that the two-phase conservation equations may be solved sequentially using commercially available software. Numerical parameters that are in a range of practical interest were determined and the numerical validation of both solvers proved to be satisfactory. Having established the robustness of the method, it could be applied to the simulation of a model restrained solidification test. It was shown that the classical hot tearing criterion approach led to complex results about the effect of notching. Moreover, it was possible to show that fracture mechanics is not the best way to consider hot tearing and that approaches based on damage formation and accumulation are more likely to be successful. In future work, more advanced criteria may be formulated based on detailed micro-scale information obtained from granular models [9].

Acknowledgments

The authors would like to thank the Commission for Technology and Innovation, CTI, Bern (Grant 6167.1) and the industrial partners Calcom-ESI (CH), Alcan (CH), Alcan (FR), HydroAluminium (DE), General Motors (USA) and Umicore (BE) for their financial support. They would also like to thank Dr O Ludwig and Dr G Couturier for their help in using the mechanical model and the porosity module, respectively.

References

[1] Suyitno, Kool W H and Katgerman L 2005 Hot tearing criteria evaluation for direct-chill casting of an Al-4.5% Cu alloy *Metall. Mater. Trans.* A **36** 1537–46

[2] Rappaz M, Drezet J-M and Gremaud M 1999 A new hot tearing criterion *Metall. Mater. Trans.* A **30** 449–55

[3] M'Hamdi M, Mo A and Martin C L 2002 Two-phase modeling directed towards hot tearing formation in aluminium direct chill casting *Metall. Mater. Trans.* A **33** 2081–93

[4] Ni J and Beckermann C 1991 A volume-averaged two-phase model for transport phenomena during solidification *Metall. Mater. Trans.* B **22** 349–61

[5] Drezet J-M, Ludwig O, M'Hamdi M, Fjaer H G and Martin C L 2004 *Light Metals* (Charlotte, North Carolina, USA: TMS)

[6] Ludwig O, Drezet J-M, Martin C L and Suéry M 2005 Rheological behavior of Al–Cu alloys during solidification: constitutive modeling, experimental identification, and numerical study *Metall. Mater. Trans.* A **36** 1525–35

[7] Rappaz M, Jacot A and Boettinger W J 2003 Last-stage solidification of alloys: theoretical model of dendrite-arm and grain coalescence *Metall. Mater. Trans.* A **34** 467–79

[8] Mathier V, Rappaz M and Jacot A 2004 Coalescence of equiaxed grains during solidification *Modelling Simul. Mater. Sci. Eng.* **12** 479–90

[9] Vernède S and Rappaz M 2006 Transition of the mushy zone from continuous liquid films to a coherent solid *Phil. Mag.* **86** 3779–94

[10] Ludwig O, Drezet J-M, Ménès P, Martin C L and Suéry M 2005 Rheological behavior of a commercial AA5182 aluminum alloy during solidification *Mater. Sci. Eng.* A **413–414** 174–9

[11] Van Haaften W M, Magnin B, Kool W H and Katgerman L 2002 Constitutive behavior of As-cast AA1050, AA3104 and AA5182 *Metall. Mater. Trans.* A **33** 1971–80

[12] Stangeland A, Mo A, Nielsen O, Eskin D and M'Hamdi M 2004 Development of thermal strain in the coherent mushy zone during solidification of aluminum alloys *Metall. Mater. Trans.* A **35** 2903–15

[13] Pequet C, Gremaud M and Rappaz M 2002 Modeling of microporosity, macroporosity and pipe-shrinkage formation during the solidification of alloys using a mushy-zone refinement method: applications to aluminum alloys *Metall. Mater. Trans.* A **33** 2095–106

[14] Couturier G and Rappaz M 2006 Effect of volatile elements on porosity formation in solidifying alloys *Modelling Simul. Mater. Sci. Eng.* **14** 253–71

[15] ABAQUS Inc. 2003 Creep and Swelling 18.2.4-8–18.2.4-9 *ABAQUS User's Manual* (Pawtuket, RI, USA: Hibbitt, Karlsson & Sorensen)

[16] Niyama E, Uchida T, Morikawa M and Saito S 1982 A method of shrinkage prediction and its application to steel casting practice *AFS Int. Cast Met. J.* **7** 52–63

[17] M'Hamdi M, Fjaer H G, Mo A, Mortensen D and Benum S 2004 *TMS*

[18] Monroe C and Beckermann C 2005 Development of a hot tear indicator for steel castings *Mater. Sci. Eng.* A **413–414** 30–6